Improving Argos Doppler Location Using Multiple-Model Kalman Filtering

Rémy Lopez, Jean-Pierre Malardé, François Royer, and Philippe Gaspar, *Member, IEEE*

***Abstract*—The Argos service was launched in 1978 to serve environmental applications, including oceanography, wildlife tracking, fishing vessel monitoring, and maritime safety. The system allows for worldwide near-real-time positioning and data collection of platform terminal transmitters (PTTs). The positioning of the PTTs is achieved by exploiting the Doppler shift in the carrier frequency of the transmitter as recorded by satelliteborne Argos receivers. Until March 15, 2011, a classical nonlinear least squares estimation technique was systematically used to estimate Argos positions. Since then, a second positioning algorithm using a multiple-model Kalman filter was implemented in the operational Argos positioning software. This paper presents this new algorithm and analyzes its performance using a large data set obtained from over 200 mobiles carrying both an Argos transmitter and a GPS receiver used as ground truth. The results show that the new algorithm significantly improves the positioning accuracy, particularly in difficult conditions (for class-A and class-B locations, in the Argos terminology). Moreover, the new algorithm enables the retrieval of a larger number of estimated positions and the systematic estimation of the location error.**

***Index Terms*—Argos system, Doppler location, interacting multiple model (IMM) Kalman filter (KF), least squares (LS) estimation, target tracking.**

I. Introduction

THE ARGOS system allows for worldwide near-real-time positioning and data collection of platform terminal transmitters (PTTs) using dedicated receivers on board a number of polar-orbiting satellites. Argos PTTs transmit short (256 b) messages at a frequency of 401.650 MHz $\pm$ 30 kHz. Positioning leverages the Doppler effect, affecting the carrier frequency of the messages recorded by any satelliteborne Argos receiver. Until March 15, 2011, a classical nonlinear least squares (LS) estimation technique was used to estimate Argos positions. This technique requires the reception of at least two messages during a single satellite pass to estimate a position and a minimum of four messages to estimate the positioning error. Experience shows that the standard deviation of the Argos positioning error typically ranges from tens of kilometers when only two or three messages are received on a satellite pass to less than 250 m in most favorable cases when a larger number of high-quality messages are received. Unfortunately, occurrences of such favorable cases are rare for some important Argos applications such as wildlife tracking. Animal tracking indeed often imposes the use of highly miniaturized PTTs at low output power in difficult environments (for example, under dense forest covers or at the surface of rough seas). Under such conditions, Argos positioning can incur large errors and thus yield trajectories with a well-visible noise.

Thus, several methods have been proposed to, *a posteriori*, reduce errors in Argos positions and thereby obtain more realistic smoothed trajectories. Some authors proposed methods rejecting unlikely locations based on the detection of abnormal velocities [1], [2], direction changes [3], or *ad hoc* trajectory smoothing techniques [4], [5]. Such methods only provide a limited handling of observation errors and no inference capability of the true trajectory. On the other hand, likelihood-based filtering approaches [6], [7] provide a methodological framework to reduce positioning errors without rejecting locations. They typically use the flexible state-space formulation in which realistic prior observation and movement models are combined with measurements so as to estimate the location and its positioning error. While the state-space approach was systematically applied to the trajectory provided by the LS processing, it can also be used to estimate PTT locations and their errors directly from Argos frequency measurements. Such a strategy has actually been devised and implemented in the operational Argos processing chain. Its results, based on a multiple-model Kalman filter (KF), have been made available to all Argos users since March 15, 2011.

This paper presents this new positioning algorithm and analyzes its performance using a large data set obtained from over 200 mobiles carrying both an Argos transmitter and a GPS receiver used as ground truth. This paper is devised to be accessible to a large spectrum of Argos users wanting to better understand the location processing. The results show that the new algorithm significantly improves the positioning accuracy, particularly in difficult conditions, i.e., when less than four messages per satellite pass are received. In addition, the new algorithm is able to estimate a position and its associated error even when a single message is received on a satellite pass, increasing the amount of distributed locations.

Notations are standard: $P(\cdot)$, $p(\cdot)$, and $E[\cdot]$ represent a probability, a probability density function (pdf), and an expectation, respectively. $\mathcal{N}(x; \bar{x}, P)$ stands for the real Gaussian

Manuscript received March 1, 2013; revised September 13, 2013; accepted September 23, 2013. Date of publication October 25, 2013; date of current version February 28, 2014.

R. Lopez is with the Collecte Localisation Satellites, 31520 Ramonville-Saint-Agne, France and was with the Laboratoire d'Analyse et d'Architecture des Systèmes, French National Center for Scientific Research (CNRS)/Université Paul Sabatier, Université de Toulouse, 31400 Toulouse, France (e-mail: rlopez@cls.fr).

J.-P. Malardé and P. Gaspar are with Collecte Localisation Satellites, 31520 Ramonville-Saint-Agne, France (e-mail: jmalarde@cls.fr; pgaspar@cls.fr).

F. Royer was with Collecte Localisation Satellites, 31520 Ramonville-Saint-Agne, France. He is now with Datasio, 31000 Toulouse, France (e-mail: froyer@datasio.com).

Color versions of one or more of the figures in this paper are available online at http://ieeexplore.ieee.org.

Digital Object Identifier 10.1109/TGRS.2013.2284293

distribution with mean $\bar{x}$ and covariance P. The transpose operator is denoted by $\cdot^{\mathrm{T}}$.

II. LS Argos Location Processing

A. Argos Location Principle

The Argos system can locate a PTT anywhere on Earth by exploiting the Doppler effect, i.e., the frequency shift induced by the relative motion between the satellite and the platform. Let $\vec{B}$ be the platform location, $\vec{V_B}$ be its velocity, $\vec{S}$ be the satellite location, and $\vec{V_S}$ be its velocity in the standard coordinate frame of WGS84 [8]. The relationship between the transmission frequency f_t of the platform and the frequency f_r received at the satellite writes as

$$\begin{aligned} f_r &= \mathcal{H}(f_t, \vec{B}, \vec{S}, \vec{V_B}, \vec{V_S}) + v \\ &= f_t \left(1 - \frac{(\vec{V_S} - \vec{V_B}) \cdot \vec{u}}{c}\right) + v \end{aligned} \tag{1}$$

with c being the speed of light, $\vec{u} = ((\vec{S} - \vec{B})/\|\vec{S} - \vec{B}\|)$ being the unitary vector directed from the platform to the satellite, and $\|\cdot\|$ being the Euclidean norm. The zero-mean Gaussian noise v captures measurement uncertainties. The scalar product $(\vec{V_S} - \vec{V_B}) \cdot \vec{u}$ accounts for the relative radial velocity between the PTT and the satellite. Since $\|\vec{V_B}\| \ll \|\vec{V_S}\| \approx 7$ km $\cdot$ s^{-1}, the platform speed is neglected in (1).

In the observation function $\mathcal{H}$, the satellite ephemeris $\vec{S}$ and $\vec{V_S}$ are given. Moreover, the platform is assumed to lie on the terrestrial reference ellipsoid of WGS84 so that $\vec{B} = \vec{B}(\lambda, \phi, h)$ with λ being the platform longitude, ϕ being its longitude, and h being its altitude. For marine platforms, the altitude over this ellipsoid is set to zero, while for terrestrial platforms and birds, the altitude is approximated by the digital terrain model GTOPO30 [9]. The remaining unknowns are the frequency f_t as well as the platform longitude λ and latitude ϕ. Henceforth, $\mathcal{H}(f_t, \vec{B}, \vec{S}, \vec{V_B}, \vec{V_S})$ will be denoted $\mathcal{H}(\lambda, \phi, f_t)$.

The frequency measurements can only be collected during *satellite passes*. A pass is the time during which a platform remains in the visibility circle of a satellite (15 min maximum). For a given PTT, measurements belonging to the same satellite pass are grouped together. These batches of frequency measurements are then processed sequentially considering that the location and the transmission frequency of the platform are fixed during a pass. The time index $k = 0, 1, \ldots$, denotes the satellite pass, and the associated location is given at the average date of the associated measurements. As the satellite position and velocity are specific to each measurement of a pass, let $\mathcal{H}_k^i$ be thereafter the Doppler function of the ith measurement of the kth pass.

Knowing the transmitting frequency, the set of possible platform locations upon receipt of one message is a curve given by the intersection of the Earth surface with a cone of apex $\vec{S}$ and axis $\vec{V_S}$. Under the assumption that there are no measurement uncertainties and with more than one message, the solution set reduces to two locations on Earth, lying at the intersection of all solution cones: the *nominal* ("true") and the *mirror* ("virtual") locations (see the example in Fig. 1 for two measurements). The two solutions are symmetrical with respect to the subsatellite track, and unfortunately, they are not *a priori* distinguishable.

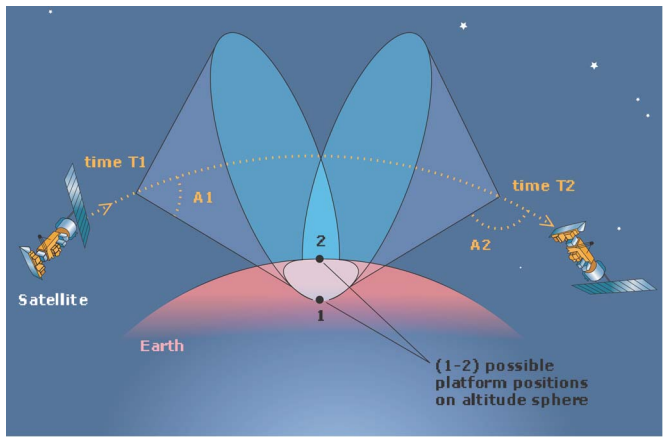

Fig. 1. Two possible Argos locations are at the intersection of Doppler solution cones with the Earth surface.

B. LS Fitting

LS problems arise in data fitting. The aim is to estimate n unknown parameters of an observation model h_k from $m_k \geq n$ imperfect measurements. Let $x_k \in \mathbb{R}^n$ be the vector of parameters and $z_k \in \mathbb{R}^{m_k}$ be the vector of observations. The system to solve writes as

$$z_k = h_k(x_k) + v_k \tag{2}$$

where $v_k \in \mathbb{R}^{m_k}$ represents a random Gaussian measurement error with known mean $\bar{v}_k = 0$ and variance R_k. The sum of the squared residuals is defined as the random variable

$$S_k(x_k) = \|z_k - h_k(x_k)\|^2_{R_k^{-1}} \tag{3}$$

with $\|U\|^2_W = U^{\mathrm{T}} W U$. The LS estimator provides the estimate $\hat{x}_k$ by minimizing the expectation of S_k with respect to x_k.

In the localization context, $x_k = (\lambda_k, \phi_k, f_{t,k})^{\mathrm{T}}$ is a vector made of $n = 3$ unknowns, and z_k is a set of m_k frequency observations. The problem of estimating the location and the transmitting frequency writes as a nonlinear equation system with $h_k(x_k) = [\mathcal{H}_k^1(x_k) \cdots \mathcal{H}_k^i(x_k) \cdots \mathcal{H}_k^{m_k}(x_k)]^{\mathrm{T}}$ and $R_k = \sigma_k^2 I_{m_k}$, where σ_k stands for the standard deviation of the measurement noise. The shape of S_k is composed of two minimums which are symmetrical about the ground track of the satellite and centered on the image and nominal positions. As the Doppler observation function h_k is nonlinear, the LS estimator has no closed-form solution. To handle nonlinearities, we proceed iteratively. The observation function is first approximated by a linear expression

$$z_k = h_k(x_k) + v_k \approx h_k\left(\hat{x}_k^0\right) + H_k^0 \delta x_k^0 + v_k \tag{4}$$

with $\hat{x}_k^0$ being an initial estimate of the true solution, $\delta x_k^0 = x_k - \hat{x}_k^0$, and $H_k^0 = (\partial h_k / \partial x_k)|_{\hat{x}_k^0} \in \mathbb{R}^{m_k \times n}$.

The squared residual becomes $S_k(x_k) \approx S'_k(\delta x_k^0) = \|z_k - h_k(\hat{x}_k^0) - H_k^0 \delta x_k^0\|^2_{R_k^{-1}}$, and its expected value reaches a minimum w.r.t. δx_k^0 at

$$\delta \hat{x}_k^0 = \left({H_k^0}^{\mathrm{T}} R_k^{-1} H_k^0 \right)^{-1} {H_k^0}^{\mathrm{T}} R_k^{-1} \left(z_k - h\left(\hat{x}_k^0 \right) \right). \quad (5)$$

Then, the next solution estimate $\hat{x}_k^1 = \hat{x}_k^0 + \delta \hat{x}_k^0$ is used as the initial guess to compute $\hat{x}_k^2$ and so on. This iterative refinement amounts to the Gauss–Newton method [10]. It is stopped at iteration j when the variation of S becomes small enough or when a maximum number of iterations are reached.

The initial position guess $(\hat{\lambda}_k^0, \hat{\phi}_k^0)$ in (4) is calculated using the geometric location principle [11, Sec. 3.2]. The geometric location computes two initial positions: the first one close to the nominal location and the second one close to the mirror location (it is not known at this stage how to distinguish them). Moreover, the initial estimate $\hat{f}_{t,k}^0$ of the frequency emitted by the PTT is its last estimated value. The aforementioned iterative refinement is then successively applied to each of the two initial estimates using all the messages of the pass, which leads to two solutions. In order to select the nominal solution and to assess its likelihood, four plausibility tests, described in [11, Sec. 3.2], are applied. If the platform is seen for the first time, no estimate of the transmission frequency is available to initialize the algorithm. In this case, the algorithm scans the frequency bandwidth by steps of 500 Hz around the average frequency of the received messages. For each frequency value, it performs the geometric location and refinement. Then, among all the resulting candidate solutions, the one with the smallest residual value is kept.

In practice, the Argos location algorithm adapts the refinement step depending on the number of measurements.

1) Computations With at Least Four Measurements: The problem is *overdetermined* because there are more measurements than unknown parameters. Thus, an LS estimate of $(\lambda_k, \phi_k, f_{t,k})^{\mathrm{T}}$ can be computed for both the nominal and mirror solutions as well as the associated covariance matrix of the error

$$\mathrm{cov}\left(x_k - \hat{x}_k^j \right) \approx \left(\hat{\sigma}_k^j \right)^2 \left({H_k^j}^{\mathrm{T}} H_k^j \right)^{-1} \quad (6)$$

with the estimated observation noise standard deviation

$$\hat{\sigma}_k^j = \sqrt{\frac{S\left(\hat{x}_k^j \right)}{m_k - n}}. \quad (7)$$

2) Computations With Three Measurements: In this case, $m = n$ and the LS method is still directly applicable. However, as the estimated observation noise in (7) is undefined, the only deliverable information about the error is the geometric dilution of precision (GDOP)

$$\mathrm{GDOP} \approx \sqrt{\mathrm{tr}\left(\left({H_k^j}^{\mathrm{T}} H_k^j \right)^{-1} |_{\lambda,\phi} \right)} \quad (8)$$

where $\mathrm{tr}(X)$ is the trace of the matrix X and $X|_{\lambda,\phi}$ is the matrix X reduced to its spatial part (λ, ϕ). The GDOP value depends on the number of messages received and how they are distributed within the satellite pass. If the observation geometry is favorable, i.e., if a plethora of messages uniformly distributed within the pass are available, the value of GDOP will be small. On the contrary, if only a few messages are recorded during a short part of the pass, the observation geometry will be bad and GDOP will take high values.

3) Computations With Two Measurements: The system is *underdetermined* with an infinite number of solutions. Hence, we consider that the transmission frequency is known and equal to its last estimate. We have to solve again a nonlinear system with as many unknowns as equations.

C. About Location Errors

An interesting point is that the errors associated with the Argos location estimates are given as an error ellipse with a semimajor axis a, a semiminor axis b, and an angle θ (from north when heading east). These quantities are derived from the covariance matrix stemming from (6) for at least four messages. For convenience only, users are also provided with an "equivalent error radius" R equal to $\sqrt{ab}$ to easily classify locations according to their accuracy. However, as errors are seldom isotropic, one must keep in mind that the equivalent error radius may not constitute a faithful characterization.

The locations are assigned a level of accuracy among seven location classes (LCs): 3, 2, 1, 0, A, B, and Z. For a satellite pass with a minimum of four messages, an error estimate can be computed and is used for the classification. Locations with an error radius under 250 m belong to LC 3, between 250 and 500 m to LC 2, between 500 and 1500 m to LC 1, and beyond 1500 m to LC 0. For a satellite pass with three or two messages, the estimated accuracy is unknown, so locations are tagged as LC A and LC B, respectively. Locations where the LS iterative refinement fails to converge are tagged as class Z.

D. Limitations of the LS Location Processing

The LS location processing has three main limitations.

1) Low Accuracy Under Difficult Conditions: While positioning errors of 250 m can be reached in best case scenarios, comparisons with GPS positions showed that many applications do not display such accurate locations [12]–[14]. For example, the oscillator's medium-term stability is strongly conditioned on the temperature gradients experienced by the PTT during a satellite pass. These phenomena lead to larger uncertainties on the estimated trajectories. They are amplified when the average number of received messages is low because measurements are less well distributed within the pass and the estimated frequency cannot be updated by the location algorithm (one falls in the case of computations with two measurements). Other sources of errors contribute to inaccuracies, such as the movement of the PTT between transmissions or ambient and ionospheric noise around the 401.650-MHz frequency.

2) Mirror Locations: The location algorithm provides two solutions and tags the most plausible one as the "nominal" location. Sometimes, the algorithm makes the wrong decision and outputs the mirror location as first solution. Mirror locations can

correspond to errors of 5000 km, which is the diameter of the visibility circle of the satellites.

3) No Error Estimation for Locations With Three or Two Messages: When the number of messages received by the satellite is lower than four, no error estimation is given. This includes locations tagged as LC A and LC B and results in the use of heterogeneous data by the users.

III. New Location Algorithm: Multiple-Model Kalman Filtering

A. KF Applied to Argos Location

The localization problem can be formulated as the estimation of the state of a dynamic system. The true state $x = (\lambda, \phi, f_t, \ldots)^{\mathrm{T}}$ of the platform includes the location, the transmission frequency, and possibly unknowns of higher order (velocity, frequency drift, ...). At initial time, the distribution of x_0 is characterized by $p(x_0) = \mathcal{N}(x_0; \hat{x}_{0|0}, \hat{P}_{0|0})$. The state dynamics $p(x_k|x_{k-1})$ is described by the Markov model

$$x_k = f_k(x_{k-1}) + w_k \tag{9}$$

with k being the time index of the satellite pass, f_k being the state transition function, and $w_k \sim \mathcal{N}(w_k; \bar{w}_k, Q_k)$ being the process noise. The observation pdf $p(z_k|x_k)$, which links the observed frequency measurements z_k with the state vector x_k through the Doppler observation function h_k, directly comes from the output equation

$$z_k = h_k(x_k) + v_k \tag{10}$$

where $v_k \sim \mathcal{N}(v_k; \bar{v}_k, R_k)$ terms the measurement noise. For (9) and (10), the sequences $\{h_\cdot, \bar{v}_\cdot, R_\cdot\}$ and $\{f_\cdot, \bar{w}_\cdot, Q_\cdot\}$ are given, and the noises w_k and v_k are assumed white, mutually independent, and independent of x_0.

The aim is to approximate over time the posterior pdf $p(x_k|z_{1:k})$ of the state x_k conditioned on the measurements $z_{1:k} = (z_1, \ldots, z_k)$. If the state and output equations (9) and (10) are linear, then under the aforementioned Gaussian assumptions, the posterior pdf $p(x_k|z_{1:k})$ is also Gaussian. It can be then reduced to its first two moments $\hat{x}_{k|k} = E[x_k|z_{1:k}]$ (equivalently the location estimate of the platform) and the posterior covariance $P_{k|k} = E[(x_k - \hat{x}_{k|k})(x_k - \hat{x}_{k|k})^{\mathrm{T}}|z_{1:k}]$ (equivalently the location error covariance) of the state x_k. In this case, the moments can be analytically determined by the KF [15]. The KF first propagates forward in time the last state estimate $\hat{x}_{k-1|k-1}$ and the last covariance estimate $P_{k-1|k-1}$ using only the prior dynamics model. The predicted mean $\hat{x}_{k|k-1}$ and covariance $P_{k|k-1}$ are then corrected considering the information brought by the measurement z_k in order to build $\hat{x}_{k|k}$ and $P_{k|k}$. The KF is an unbiased estimator and computes also the minimum mean-square error estimate as it minimizes the expectation $E[\|x_k - \hat{x}_{k|k}\|^2] = \mathrm{tr}(P_{k|k})$.

The KF has proved particularly fruitful in target tracking and was originally designed for linear systems, but several extensions have been proposed to handle nonlinearities. The widespread extended KF [16] propagates the posterior covariances by performing a first-order Taylor expansion of the transition/measurement models around the most recent estimate/prediction of the state. More recently, the unscented KF [17], [18], which performs a statistical linearization based on the sigma-point (or unscented) transformation [19], was proved to give better results, in both theory and practice. For numerical issues, we use its square root implementation [20].

Compared with LS fitting, calculations can be made regardless of the number of measurements and enable a systematic characterization of the estimation error through the posterior covariance $P_{k|k}$. Concretely, location estimates calculated with three and two messages (tagged as classes A and B, respectively) are associated with an error covariance, and locations computed from the reception of a single message can now be computed (tagged as class B too). The filter outputs a unique solution. Moreover, there is no need to assume that the transmission frequency remains identical between two consecutive satellite passes when less than three messages are recorded. As previously, the location is tested to check its likelihood before being distributed to Argos users.

B. Bank of KFs: Multiple-Model Approach

Kalman filtering requires prior knowledge on how a location at time k relates to a location at time $k+1$. As Argos is used to track a wide variety of mobiles, one cannot be very specific about this relation (the so-called dynamical model), and the most sensible is to assume that λ and ϕ undergo a random walk. Movement models based on a random walk process and its variations have been extensively developed in [21] for biological applications. As for the frequency, a major assumption of the Argos system is that the PTT's internal oscillator frequency is stable over time, provided that the ambient temperature does not vary too much. Thus, the frequency is assumed identical on average between two consecutive locations whatever the motion model but is affected by an additive stationary noise V_f which captures the effects due to temperature gradients. The complete dynamical model thus reads as

$$x_k = x_{k-1} + w_k \tag{11}$$

where

$$\bar{w}_k = 0 \qquad Q_k = \begin{pmatrix} 2D_\lambda \Delta t_k & 0 & 0 \\ 0 & 2D_\phi \Delta t_k & 0 \\ 0 & 0 & V_f \end{pmatrix} \tag{12}$$

with $\Delta t_k = t_k - t_{k-1}$ being the elapsed time since the previous satellite pass and $x_k = (\lambda_k, \phi_k, f_{t,k})^{\mathrm{T}}$. The diffusion parameters of the random walk are $D_\lambda = D_\phi = D$. The 1σ probability surface of the next platform location x is proportional to $2D\Delta t_k$.

Directed movements of the platforms are well modeled with a correlated random walk (CRW) which is a random walk on the velocity. The corresponding dynamic model writes as

$$x_k = \begin{pmatrix} 1 & 0 & \Delta t_k & 0 & 0 \\ 0 & 1 & 0 & \Delta t_k & 0 \\ 0 & 0 & 1 & 0 & 0 \\ 0 & 0 & 0 & 1 & 0 \\ 0 & 0 & 0 & 0 & 1 \end{pmatrix} x_{k-1} + w_k \tag{13}$$

where

$$\bar{w}_k = 0 \qquad Q_k = \begin{pmatrix} 0 & 0 & 0 & 0 & 0 \\ 0 & 0 & 0 & 0 & 0 \\ 0 & 0 & 2D'_\lambda \Delta t_k & 0 & 0 \\ 0 & 0 & 0 & 2D'_\phi \Delta t_k & 0 \\ 0 & 0 & 0 & 0 & V_f \end{pmatrix}$$

assuming that $x_k = (\lambda_k, \phi_k, v_{\lambda,k}, v_{\phi,k}, f_{t,k})^{\mathrm{T}}$ where $v_k = (v_\lambda, v_\phi)$ stands for the velocity of the platform. On the basis of this model, the next position and velocity can be predicted from the last estimation of the platform position and velocity.

Of course, a single random walk or CRW cannot perfectly capture all platform behaviors. A better model would consider switches between multiple behaviors: A ship can conduct fishing operations and then steam back to port, while a marine mammal can reside in wintering grounds for several months before migrating to new locations. As such, observed velocities can vary by an order of magnitude along the track, inducing changes in the temporal correlation and breakage of the Markovian property in the single-model approach.

Multiple-model filtering through a bank of KFs is suitable to handle multiple hypotheses (or *modes*) when assimilating measurements. The discrete-time jump Markov system takes the form of a dynamic system. The mode in effect during the sampling period $(t_{k-1}, t_k]$ is represented by the discrete random index m_k and takes on a value within a given set $\mathcal{M}$ of cardinality M. The sequence of random variables $m_0, m_1, m_2, \ldots$, follows a homogeneous finite-state Markov chain with

$$\forall\,(i,j) \in \mathcal{M} \times \mathcal{M},\ P(m_k = i | m_{k-1} = j) = \pi_{ji}. \tag{14}$$

At initial time, the distribution of x_0 is characterized by $p(x_0) = \sum_{m_0 \in \mathcal{M}} P(m_0) p(x_0|m_0)$, where

$$P(m_0 = i) = \mu_0^i \qquad p(x_0|m_0 = i) = \mathcal{N}\left(x_0; \hat{x}_{0|0}^i, P_{0|0}^i\right) \tag{15}$$

and the statistics μ_0^i, $\hat{x}_{0|0}^i$, and $P_{0|0}^i$ are given. The transition pdf between times $k-1$ and k is assumed to write as $p(m_k, x_k | m_{k-1}, x_{k-1}) = P(m_k|m_{k-1}) p(x_k|m_k, x_{k-1})$. Conditionally, on the active mode m_k over $(t_{k-1}, t_k]$, the assumed base state dynamics $p(x_k|m_k = i, x_{k-1})$ follows from the state equation

$$x_k = f_k^i(x_{k-1}) + w_k^i, \qquad w_k^i \sim \mathcal{N}\left(w_k^i; \bar{w}_k^i, Q_k^i\right) \tag{16}$$

where the dynamics noise w_k^i is white and independent of x_0^i and where $\{f^i, \bar{w}^i, Q^i\}_{i \in \{1,\ldots,M\}}$ is given. Similarly, the observation pdf $p(z_k|m_k = i, x_k)$, which unites the state vector and the measurement z_k under the assumption that $m_k = i$, straightly comes from the output equation

$$z_k = h_k^i(x_k) + v_k^i, \qquad v_k^i \sim \mathcal{N}\left(v_k^i; \bar{v}_k^i, R_k^i\right) \tag{17}$$

where the measurement noise v_k^i is white and independent of x_0^i and where $\{w_l^i\}_{l \in \{1,\ldots,k-1\}}$ and $\{h^i, \bar{v}^i, R^i\}_{i \in \{1,\ldots,M\}}$ are given.

In the framework of discrete-time jump Markov systems, the pdf $p(x_k|z_{1:k})$ writes as a Gaussian mixture with M^{k+1} components [22]

$$p(x_k|z_{1:k}) = \sum_{i_{0:k} \in \mathcal{M}^{k+1}} p(x_k|m_{0:k} = i_{0:k}, z_{1:k}) \times P(m_{0:k} = i_{0:k}|z_{1:k}) \tag{18}$$

where $i_{0:k} = \{i_0, \ldots, i_k\}$ is a sample of the model sequence $m_{0:k} = \{m_0, \ldots, m_k\}$ from time 0 to k. The exponentially growing complexity of the problem precludes an exact resolution. The interacting multiple model (IMM) algorithm has become a standard approach to derive a tractable solution by merging the growing tree of model sequences. On the basis of the sequence of measurements $z_{1:k} = (z_1, \ldots, z_k)$, the IMM propagates along time a Gaussian approximation $\mathcal{N}(x_k; \hat{x}_{k|k}^i, P_{k|k}^i)$ of the posterior density $p(x_k|m_k = i, z_{1:k})\ \forall\, i \in \mathcal{M}$ (where $\hat{x}_{k|k}^i$ is the posterior estimate and $P_{k|k}^i$ is the posterior covariance matched to mode i) and the posterior mode probability $P(m_k|z_{1:k})$. The IMM filter was first outlined in [23] and is surveyed with alternative multiple-model strategies in [22].

C. Building a Set of Dynamic Models

Our aim is to make random walks with state vector $x = (\lambda, \phi, f_t)^{\mathrm{T}}$, and CRWs with state $x = (\lambda, \phi, v_\lambda, v_\phi, f_t)^{\mathrm{T}}$ cooperate inside an IMM filter. Nevertheless, the standard IMM filter is not fully adapted to handle a bank of mode-matched filters with state vectors of heterogeneous size and meaning. To circumvent the use of heterogeneous-order state-space models, a random walk with a time-dependent bias term is considered instead of a CRW. The complete dynamical model, with $x_k = (\lambda_k, \phi_k, f_{t,k})^{\mathrm{T}}$, writes as

$$x_k = x_{k-1} + \begin{pmatrix} \hat{v}_{k|k-1} \Delta t_k \\ 0 \end{pmatrix} + w_k \tag{19}$$

$$\bar{w}_k = 0 \qquad Q_k = \begin{pmatrix} 2D_\lambda \Delta t_k & 0 & 0 \\ 0 & 2D_\phi \Delta t_k & 0 \\ 0 & 0 & V_f \end{pmatrix}.$$

The predicted velocity $\hat{v}_{k+1|k}$ to be used in the time update at time $k+1$ prior to assimilating the measurement z_{k+1} is computed separately with an exponential moving average such as

$$\hat{v}_{k+1|k} = \alpha \tilde{v}_k + (1 - \alpha) \hat{v}_{k|k-1} \tag{20}$$

where $\alpha = 0.3$ and $\tilde{v}_k$ terms an approximate empirical velocity defined as

$$\tilde{v}_k = \frac{(\lambda_k, \phi_k)^{\mathrm{T}} - (\lambda_{k-1}, \phi_{k-1})^{\mathrm{T}}}{\Delta t_k}. \tag{21}$$

With this value of α, the weight of the five most recent velocity observations used by the exponential moving average is about 86% of the total weight. The estimated velocity $\hat{v}_{k+1|k}$ is smoothed to lower the erratic behavior of the finite-difference estimation that is generally observed on raw Argos data. During directed movement, the IMM is intended to switch to this additional mode. For all modes, the transmitted frequency

TABLE I
LIST AND CHARACTERISTICS OF THE PTTS INCLUDED IN THE DATA SET

Type of mobile	Number of platforms	Number of locations			Data owner and references
		LS	KF	GPS	
Marabou stork *Leptoptilos crumeniferus*	5	3 472	3 759	8 250	Neil and Liz Baker (Tanzania Bird Atlas, P.O. Box 1605, Iringa, Tanzania)
Geese *Anser indicus*	55	16 097	21 220	80 980	Lucy Hawkes (University of Exeter, Penryn Campus, Cornwall, TR10 9EZ, UK), Charles Bishop (Bangor University, Bangor, Gwynedd, LL57 2DG, UK) and Pat Butler (University of Birmingham, Birmingham, B15 2TT, UK) [25]
Blue wildebeest *Connochaetes taurinus*	10	2 029	2 180	4 144	Moses Selebatso (Western Kgalagadi Conservation Corridor Project)
Bighorn *Ovis canadensis*	13	1 819	2 159	1 704	Norv Dallin (Nevada Department of Wildlife, Eastern Region - 60 Youth Center Drive – 89801 Elko – NV, USA)
Flatback Turtle *Natator depressus*	19	16 879	24 205	21 809	Kellie Pendoley (Pendoley Environmental Pty Ltd, 2/1 Aldous Place, Booragoon, WA 6154)
Green Turtle *Chelonia mydas*	24	8 690	15 959	13 340	Simon Benhamou (Centre d'Ecologie Fonctionnelle et Evolutive, U.M.R. 5175 Montpellier, France) [26]
Galapagos Sea Lion *Zalophus wollebaeki*	9	1 224	1 680	3 027	Daniel Costa (Department of Ecology and Evolutionary Biology Institute of Marine Sciences, Long Marine Lab University of California, Santa Cruz Santa Cruz, California, USA) [27]
Elephant Seal *Mirounga angustirostris* *Mirounga leonina*	26	6 305	13 120	62 664	- Daniel Costa [28] - Christophe Guinet (Centre d'Etudes Biologiques de Chizé, 79360 Villiers-en-Bois, France) [29], [30]
Ship	23	20 160	23 404	36 425	Various
Drifter	44	48 733	54 817	175 633	Luca Centurioni (Scripps Institution of Oceanography, Physical Oceanography Research Division, 9500 Gilman Drive, Mail Code 0213, La Jolla, CA, 92093 USA)
Total	**228**	**125 408**	**162 503**	**430 370**	

noise covariance V_f equals 100 Hz^2 to handle most common temperature gradients, the standard deviation of the noise on each measured frequency is set to 0.4 Hz (deduced from the short-term stability of the embedded clock of the satellite), and the diffusion parameter D is tuned by incremental research.

D. Dealing With Location Ambiguity

As IMM filtering is a recursive process, it needs a prior initial estimate $\hat{x}^i_{0|0}$ and covariance $P^i_{0|0}$ for all mode i in $\mathcal{M}$. For this, an LS analysis is performed on the basis of at least four measurements so as to compute the initial state and covariance common to all modes. However, the LS filter systematically produces a nominal and mirror location which cannot be distinguished at the first satellite overpass. This ambiguity is solved during the next pass by applying successively one instance of the IMM filter on both locations and by selecting the one with the highest overall likelihood $L_k = \sum_i p(z_k|m_k = i, z_{1:k-1})P(m_k = i|z_{1:k-1})$ [24].

The algorithm is endowed with the ability to detect tricky cases through plausibility checks, such as frequency jumps, wrong ambiguity resolution, or fast platform transportation. When a location does not pass the plausibility checks, the algorithm attempts an automatic and instantaneous reset using an LS analysis so that the filtering process can continue seamlessly in the next satellite overpass. If this last LS adjustment fails, the location estimate is invalidated and tagged as class Z.

Although a KF provides only one location estimate, it is legitimate to wonder why it should always be the nominal one. With the traditional LS method, it is possible to fully remove the mirror location by mixing measurements from several satellite passes. This requires gathering frequency measurements close in time, i.e., within less than half an hour. Beyond 30 min, the calculation is hazardous because the platform may have moved significantly. From a geometrical point of view, the platform has to be simultaneously in the visibility circle of several satellites, a situation that occurs frequently at high latitude (20% of probability) but more rarely near the equator. The existence of at least two points of view removes the mirror solution. In comparison, the KF introduces a direct link between locations through the prior dynamics. The effect of this model is twofold: It creates a mathematical relationship between two successive satellite passes, and it captures the admissible displacements of the platform. Thus, the point of view of the last pass is shared through the last location estimate and, mainly, through the posterior covariance matrix. Additionally, the prior dynamics model modifies them depending on the elapsed time. The shape of the error ellipse (flatness and orientation), derived from the covariance matrix, is indeed highly constrained by the relative position of the satellite and the platform. Thus, the KF recreates the conditions of multipass processing.

IV. VALIDATION OF THE NEW LOCATION ALGORITHM

A. Data Set

The behaviors of the LS and of the multiple-model KF Argos positioning algorithms have been compared using a large data set including over 200 PTTs deployed on animals (birds and terrestrial and marine animals), ships, and drifting buoys. These platforms cover a wide range of geographic areas, admissible movements, and PTT types. Moreover, they are all equipped with a GPS receiver. The GPS positions, whose errors seldom exceed few tens of meters, have been used as ground truth to empirically characterize the error in the Argos positions. The frequency measurements and the corresponding satellite

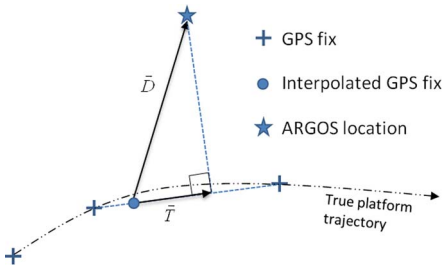

Fig. 2. Error is the distance between an Argos location and the corresponding interpolated GPS, i.e., the modulus of vector $\vec{D}$. The tangential error is the orthogonal projection of $\vec{D}$ onto the straight line connecting two GPS fixes surrounding the interpolated GPS location, i.e., the modulus of vector $\vec{T}$.

positions were provided to the LS and KF positioning algorithms to produce two sets of location estimates for each tested PTT. These two sets include all positions except the class-Z ones. Both data sets include well over 100 000 location estimates (see Table I). Since the reprocessing of the trajectories was done offline, from several days to several months after the acquisition of data, the available estimates of the orbit parameters were slightly more accurate than the estimates available in real time.

The GPS positions of all PTTs of the data set were extracted from the corresponding Argos messages. As GPS and Argos dates do not generally match with each other, the GPS locations were linearly interpolated to those of Argos. The interpolated GPS locations were then considered as the genuine locations, as done in previous studies of Argos location accuracy (e.g., [13] and [14]). The empirical error on an Argos location was set to its estimated distance to the corresponding interpolated GPS fix, i.e., the modulus of vector $\vec{D}$ in Fig. 2. Thus, it includes the small GPS positioning error and the interpolation error. To minimize the latter, only Argos locations obtained within 15 min of a GPS position were considered. This maximum accepted time difference was increased to 1 h for the slowly moving wildebeests and bighorns for which there are relatively little data. No other data removal, nor filtering, was performed on the Argos or GPS data in order to get the empirical errors and compare them with the error statistics produced by the LS and KF algorithms.

The number of Argos locations finally selected for comparison with GPS is detailed in Table II. The comparison data set still contains over 70 000 locations for both LS and KF, thereby providing a solid basis for evaluating the accuracy of Argos locations. Only a few data subsets, namely, the marabou stork, wildebeest, and bighorn sets of location estimates with less than four messages, contain less than 100 records and thus may yield less reliable statistics.

B. Number of Retrieved Positions

Interestingly, Table I shows that Kalman filtering produces about 30% more positions than LS processing. However, this increase in the number of positions is not homogeneously distributed over all PTTs in the data set (see Fig. 3). The number of positions retrieved for elephant seals and flatback turtles is nearly doubled. The number of positions is also markedly increased for sea lions (+37%) and geese (+32%). The gain is more limited (below 20%) for all other PTTs. Most (88%) new KF positions actually correspond to one-message locations, with the rest being LS class-Z positions that are now successfully estimated by the KF. The capability to estimate a position from a single message clearly benefits to marine animals for which the number of messages transmitted during one surfacing event is generally small (see Table II). Similarly, the capability to estimate positions from a single message benefits to geese that were tracked migrating between Mongolia and India, a region where the electromagnetic noise in the Argos frequency band is specially high and reduces the number of messages transmitted during one satellite pass.

C. Location Error Reduction

To better characterize the data set, six indicators were selected describing the quality of the transmitted signal, plus two indicators characterizing the movements of the tracked mobile: recorded message number, time gap between two consecutive locations, level of received signal, signal-to-noise ratio, GDOP, platform velocity, (absolute) frequency drift, and turning angle. The turning angle is the angle between the two segments connecting three consecutive locations. The mean values of these indicators are given in Table III for each type of mobile in the data set. For each statistics, the smallest value(s) of the mean is (are) colored in green, and the biggest value(s) is (are) colored in blue. These are most helpful to analyze the positioning errors for the different types of PTTs presented in Fig. 4(a) and (b). To reduce the influence of outliers in the sample (mirror locations and GPS fixes with bit errors), only the values below the 95th percentile of the error distribution have been taken into account to compute the mean errors presented in these two figures (and the corresponding standard deviations).

Fig. 4(a) shows the mean location errors obtained when at least four messages are available for positioning. With both LS and KF positioning algorithms, these errors are relatively small, ranging from about 3 km to less than 500 m. The error reduction obtained with KF is well marked only for elephant seals, flatback turtles, and ships (up to 32% of reduction), while it is small for all other types of mobiles. This was expected as this only concerns well-observed positions (greater than or equal to four messages). The information carried by the frequency observations largely dominates the position estimation, and the simple movement models included in the KF bank can hardly improve the situation. The KF however has a more positive impact on the standard deviation of the positioning error (up to 47% of reduction, compared to LS). In addition, analysis of Fig. 4(a) together with Table III unsurprisingly confirms that mobiles with low GDOP values, powerful and stable transmitters, and relatively low velocities are always better localized than mobiles displaying high GDOPs (e.g., elephant seals) or large frequency drifts (e.g., marabou storks). Geese equipped with drifting transmitters in a region of high ambient electromagnetic noise are in a most unfavorable situation.

Fig. 4(b) presents the results obtained for all locations estimated using only one, two, or three messages. In this case, where measurements are more irregularly distributed within

TABLE II
MAXIMUM TIME GAP BETWEEN AN ARGOS LOCATION AND THE NEAREST GPS LOCATION. NUMBERS OF ARGOS LOCATIONS SELECTED FOR ERROR CALCULATIONS

Type of mobile	Max. GPS gap (min)	4 messages or more		2 or 3 messages		1 message	Total (% of locations kept from Table I)	
		LS	KF	LS	KF	KF	LS	KF
Marabout	15	378	381	53	53	22	431 (12%)	456 (12%)
Geese	15	3062	3155	1223	1331	550	4285 (27%)	5036 (24%)
Blue Wildebeest	60	399	415	38	38	10	437 (22%)	463 (21%)
Bighorn	60	306	323	94	94	23	400 (22%)	440 (20%)
Flatback Turtle	15	972	1025	2390	2557	1316	3362 (20%)	4898 (20%)
Green Turtle	15	835	841	1541	1584	1145	2376 (27%)	3570 (22%)
Galapagos Sea Lion	15	207	212	176	182	101	383 (31%)	495 (29%)
Elephant Seal	15	455	482	3054	3336	3420	3509 (56%)	7238 (55%)
Ship	15	12134	12381	5213	5314	1924	17347 (86%)	19619 (84%)
Drifter	15	30009	30381	11651	11779	4170	41660 (85%)	46330 (85%)
Total		**48757**	**49596**	**25433**	**26268**	**12681**	**74190 (59%)**	**88545 (54%)**

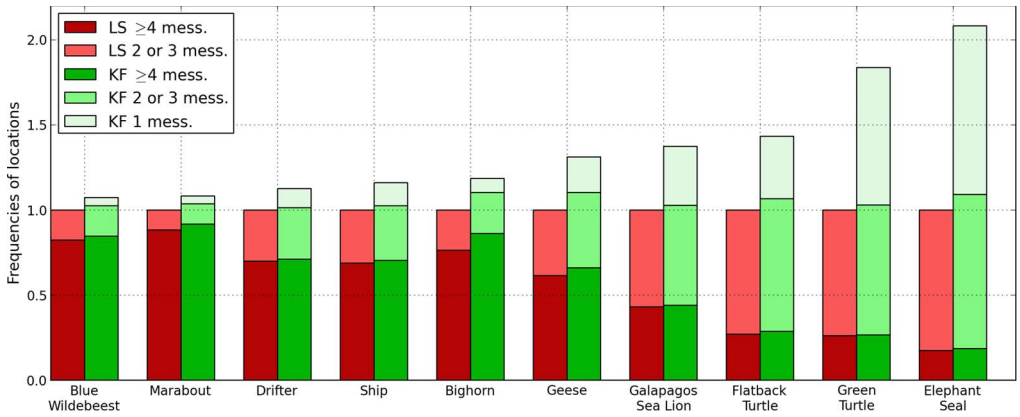

Fig. 3. Frequencies of locations w.r.t. the number of recorded messages within the satellite pass (LS processing taken as reference).

TABLE III
AVERAGE VALUES OF THE PTT TRAJECTORY STATISTICS (HIGHER VALUES ARE COLORED IN BLUE, AND LOWER VALUES ARE COLORED IN GREEN)

Type of mobile	Message number	Time between two passes (hour)	Signal level (dBm)	Signal to noise ratio (dB-Hz)	GDOP ($m.Hz^{-1}$)	Velocity ($m.s^{-1}$)	Transmitting frequency drift ($Hz.min^{-1}$)	Turning angle (deg)
Marabout	7.4	10.1	-127	43	985	1.6	0.32	108
Geese	3.7	9.9	-125	38	3640	1.94	0.31	105
Blue Wildebeest	5.3	12	-125	44	990	0.46	0.19	108
Bighorn	5.4	13.4	-129	42	1680	0.3	0.06	106
Flatback Turtle	2.6	2.7	-127	45	4242	0.58	0.08	86
Green Turtle	2.2	2.6	-129	42	4921	0.65	0.06	74
Galapagos Sea Lion	3.1	2.5	-127	44	2588	0.97	0.2	101
Elephant Seal	2.0	4.7	-131	41	6802	1.48	0.19	72
Ship	4.5	0.9	-119	47	874	2.84	0.26	62
Drifter	4.3	0.9	-119	43	720	0.55	0.05	66

the pass, the benefits of the KF are obvious. For estimations from two or three messages, the mean error of KF position is reduced between 30% (drifters) and 78% (elephant seals). In the same manner, standard deviations are reduced up to 90%. Thus, the KF approach contributes to a better accuracy and a lower dispersion of the errors, which means fewer outliers. For one-message locations, the mean errors and the standard deviations are under 10 km, which is better than the error of locations computed with two and three messages with the LS analysis. From a broader point a view, Kalman filtering is very efficient when the observation geometry is bad: Unfavorable observation geometry is indirectly supplemented by the new observation angle introduced by the last known location of the dynamics model.

A striking but common example of animal is presented in Fig. 5 for an elephant seal (*Mirounga leonina*) tracked from October 2009 to January 2010 in a round trip of approximately 3800 km near the Kerguelen Islands. Elephant seals are seagoing and migrating animals whom the large nose of the adult males looks like an elephant's trunk. The platform is localized six times per day with two messages per pass on average. An amount of 57% of the satellite passes contain two or three messages, and 38% contain only one message. In comparison to Galapagos sea lions, elephant seals spend short time at the surface and make long dive intervals [13], which limits transmission opportunities. This kind of platform benefits greatly of the advantages of the new processing: One-message satellite passes add numerous points in the trajectory with an

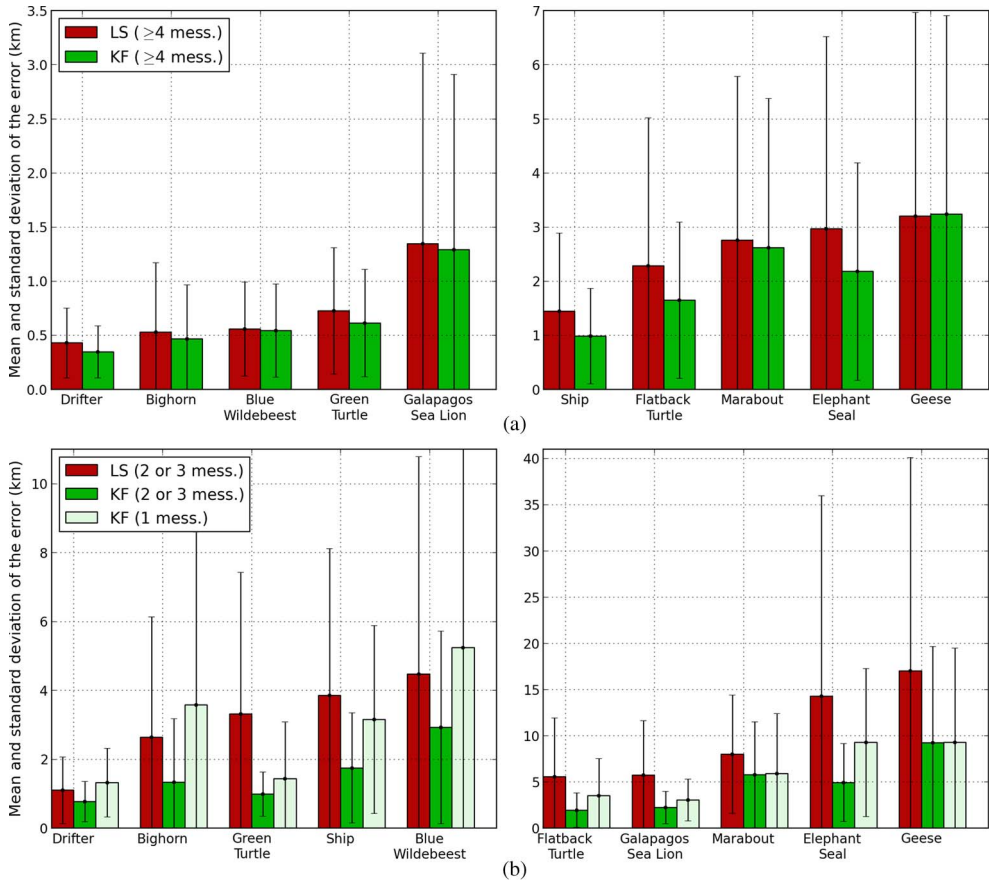

Fig. 4. Mean and standard deviation of the errors (a) with at least four messages and (b) with less than four messages (the data set is ordered by increasing LS average errors).

accuracy under 10 km (better than LS processing with two or three messages), an error estimate is provided for all locations of the track, and the overall location error is reduced from 12 to 4.5 km (-63%). For the LS algorithm, the computation of the frequency is all the more rare as the average number of messages gets low (see Section II-B). The emitting frequency is indeed assumed known and is equal to the last computed value when two messages are available. A bias on the emitting frequency increases the latitudinal error of 0.3 km per Hz of bias (the longitudinal error is negligible). One must keep in mind that daily frequency variations can reach up to 300 Hz for some platforms (due to ambient temperature variations for instance). This prevents the processing to adjust correctly the platform position with a recent emitting frequency and generates error peaks around the trajectory. Biggest outliers (sometimes falling out of the frame) result from a frequent bad choice between the nominal and mirror locations. With Kalman filtering, the use of the state-space formulation including a bank of simple dynamics models on the position and emitting frequency helps to overcome these flaws.

D. Location Error Analysis

Additional statistics on the (signed) longitudinal and latitudinal error distributions for the LS and KF algorithms are given in Tables IV and V, respectively. The longitudinal error is wider than the latitudinal one, and the error distributions are centered. The correlation coefficients between the two dimensions of the error are besides small. The major component of the Argos error is, in fact, perpendicular to the subsatellite ground track (north–south orientation). The frequencies of errors falling within the 1σ and 3σ ellipses of a Gaussian distribution with the same mean and covariance parameters indicate that the Argos error distribution is nonnormal for both methods. The observed probability of falling within the 1σ ellipse is actually much higher than the expected values (39.2%), while on average, 94% of errors are inside the 3σ ellipse (against 98.9% expected). This shows that most errors are concentrated under 1σ (the distribution has a peak around zero) but with a heavy tail due to frequent outlier values (unfavorable satellite observation geometry). This was already noticed concerning the LS method in [13], which stated that the location error distribution is nonnormal and right skewed. Study [31] suggested modeling it with Student's t distribution.

The empirical errors parallel to the platform trajectory are computed by evaluating the modulus of $\vec{T}$ which is the projection of $\vec{D}$ on the axis tangent to the GPS trajectory. The sign of the so-called tangential error is positive if the direction of $\vec{T}$ matches the trajectory direction and negative if otherwise (see Fig. 2). These computations aim at measuring a potential bias along the track due to the use of the random walk model. They are compared to the LS processing which is supposed to be unbiased. Similar to the error modulus statistics, the signed values under the 25th per mille and beyond the 975th per mille are

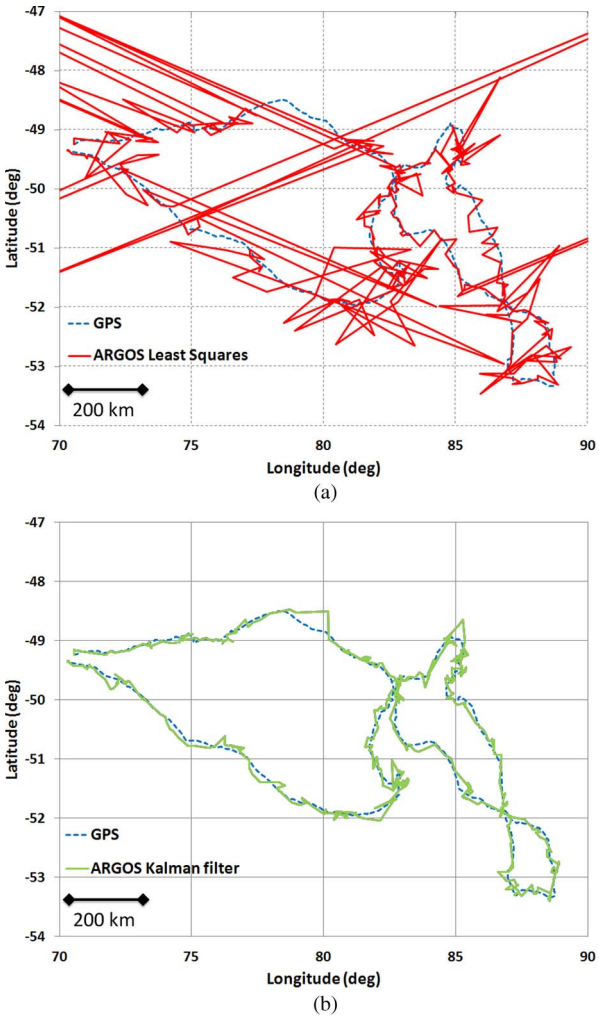

Fig. 5. Comparison of elephant seal tracks between GPS, LS, and KF. (a) GPS and LS (locations with two messages or more). (b) GPS and KF (locations with one message or more).

removed. The signed mean of these errors is given in Table VI. A negative value may indicate a systematic lag, and a positive value may indicate an advance. The part of the tangential error in the total error is limited for Kalman filtering. Its value grows slowly on average as the number of messages decreases and is generally negatively signed. The measurement update of the filter assimilates few received measurements so that the location estimation is close to the prediction. In this situation and when the random walk is the most likely dynamics, the estimated location tends to be slightly attracted by the last one. In the case of drifters, the phenomenon is more pronounced as the last computed position displays generally a very low error (a few hundreds of meters). Other outliers are observed for blue wildebeests (-45% with two or three messages in LS) and marabou storks ($+38\%$ with one message in KF), but the size of the data set is too small to draw trustworthy conclusions.

The 1σ, $\sqrt{2}\sigma$, and 3σ confidence ellipses estimated by the algorithms—containing in theory 39.3%, 63.2%, and 98.9% of the computed locations, respectively—are now considered. The $\sqrt{2}\sigma$ ellipse corresponds to that provided in Argos standard products. For a given confidence ellipse, the frequency at which position estimates actually fall within is presented in Table VII and compared to the theoretical probability. The comparison is done on all locations where a confidence ellipse is available (i.e., locations with four messages or more for LS and all locations for KF). Table VII clearly shows that the percentages of KF and LS positions falling into the different error ellipses are close to each other but systematically lower than the theoretical values. This indicates that both the LS and KF algorithms underestimate the actual positioning error, a fact that was already well known for LS, particularly in the animal tracking community (e.g., [13]). The origin of this error underestimation is twofold. First, the errors are nonnormally distributed, as discussed in the previous section. Second, unlike that assumed in (1), the frequency measurement noise is not constant but depends on factors such as the transmitter individual frequency stability, its sensitivity to temperature changes and the actual temperature changes experienced by the beacon, the platform velocity, or the ambient electromagnetic noise level in the Argos frequency band at the beacon position. Accordingly, Table VII clearly shows that the slowly moving drifters have error statistics closer to theoretical values than all other beacons as they use very stable oscillators transmitting at high output power in open ocean areas with relatively low ambient electromagnetic noise. To obtain more consistent larger KF positioning errors, one might slightly increase the assumed (constant) process and measurement noises. The problem is that no single noise estimation will work for all beacons. For example, a noise level tuned to provide accurate error ellipses for bird-tracking beacons in electromagnetically polluted areas would inevitably yield overestimated errors for drifter positions. Furthermore, individual calibration of the positioning algorithm for all transmitters and all transmission conditions is clearly out of reach. The choice has thus been made to keep the present calibration of the KF algorithm as, for all beacons tested in this paper, it reduces the actual Argos positioning errors compared to LS, even if the estimated errors remain too small as is also the case with LS. However, no other calibration of the KF algorithm in its present form would be globally satisfactory as different transmitters in different transmission conditions generate different frequency measurement errors and are thus positioned with different error levels.

V. Conclusion and Future Work

The improvements brought by the multiple-model Kalman filtering method are significant when messages are irregularly distributed within the pass and when their number is low. Kalman filtering helps to remove mirror locations and to characterize errors associated with locations estimated with less than four messages. Over the total number of locations tested, the mean error is reduced by 10% to 63%. The overall dispersion decreases from 15% to 78% so that the majority of outliers are corrected. Most of the new positions come from one-message locations which have an accuracy comparable to that of LS with less than four messages. For low-power transmitters or applications deployed in worse environmental conditions, these new locations may be of high interest.

Future work will concentrate on improving the multiple-model approach in two ways. First, by following the

TABLE IV
AVERAGE VALUES, STANDARD DEVIATIONS (SD), AND CORRELATION COEFFICIENTS OF LS ALGORITHM ERRORS (IN METERS). FREQUENCIES (IN PERCENT) OF ERRORS INSIDE THE 1σ AND 3σ ELLIPSES OF THE CORRESPONDING 2-D GAUSSIAN DISTRIBUTIONS (39.2% AND 98.9% EXPECTED RESPECTIVELY)

Type of mobile	Longitude error		Latitude error		Corr.	Freq. within:	
	Mean	(SD)	Mean	(SD)		1σ ellipse	3σ ellipse
Marabout	-327	(3457)	69	(3574)	0.12	67.7	92.9
Geese	-89	(8981)	40	(5347)	-0.08	71.4	94.1
Blue wildebeest	-127	(746)	2	(440)	0.10	61.4	96.2
Bighorn	-1	(1352)	-188	(1397)	0.38	79.0	95.8
Flatback Turtle	-158	(5984)	-213	(3936)	-0.05	72.4	93.1
Green Turtle	31	(3058)	66	(2136)	0.04	76.2	93.0
Galapagos Sea Lion	51	(4355)	498	(3196)	-0.13	73.4	93.3
Elephant Seal	362	(19201)	53	(10289)	0.04	76.7	94.3
Ship	31	(2392)	-2	(1688)	0.04	65.2	94.5
Drifter	31	(622)	-41	(481)	0.03	63.5	94.4

TABLE V
AVERAGE VALUES, STANDARD DEVIATIONS (SD), AND CORRELATION COEFFICIENTS OF KF ALGORITHM ERRORS (IN METERS). FREQUENCIES (IN PERCENT) OF ERRORS INSIDE THE 1σ AND 3σ ELLIPSES OF THE CORRESPONDING 2-D GAUSSIAN DISTRIBUTIONS (39.2% AND 98.9% EXPECTED RESPECTIVELY)

Type of mobile	Longitude error		Latitude error		Corr.	Freq. within:	
	Mean	(SD)	Mean	(SD)		1σ ellipse	3σ ellipse
Marabout	-333	(3335)	-22	(3007)	0.11	68.1	93.8
Geese	-251	(6667)	-24	(4513)	-0.04	67.0	93.5
Blue wildebeest	-87	(712)	16	(470)	0.12	64.1	95.8
Bighorn	-32	(886)	-82	(686)	-0.16	78.0	95.1
Flatback Turtle	-77	(2361)	-183	(1793)	-0.03	57.7	95.3
Green Turtle	-34	(2049)	36	(1602)	0.01	65.5	93.4
Galapagos Sea Lion	-185	(3105)	134	(2284)	-0.07	71.3	92.5
Elephant Seal	283	(7554)	-124	(4929)	-0.04	62.4	94.1
Ship	0	(1787)	-4	(1251)	0.01	65.1	94.1
Drifter	18	(516)	-37	(433)	-0.01	62.0	94.2

TABLE VI
RATIO OF THE SIGNED TANGENTIAL ERROR ON THE ERROR MODULUS

Type of mobile	4 mess. or more		2 and 3 mess.		1 mess.
	LS	KF	LS	KF	KF
Marabout	5%	1%	5%	12%	38%
Geese	2%	4%	0%	-2%	-8%
Blue Wildebeest	-1%	3%	-45%	-16%	-25%
Bighorn	-1%	-2%	19%	7%	-19%
Flatback Turtle	-5%	-13%	1%	-9%	-14%
Green Turtle	10%	5%	8%	-15%	-22%
Galapagos Sea Lion	9%	11%	13%	-7%	-2%
Elephant Seal	7%	-2%	-3%	-8%	-18%
Ship	1%	-3%	1%	-25%	-25%
Drifter	0%	-14%	2%	-38%	-60%

TABLE VII
PROBABILITIES THAT COMPUTED LOCATIONS FALL WITHIN THE ERROR ELLIPSES (HEADERS CONTAIN THE THEORETICAL VALUES)

Type of mobile	1σ (39.3%)		$\sqrt{2}\sigma$ (63.2%)		3σ (98.9%)	
	LS	KF	LS	KF	LS	KF
Marabout	14%	14%	27%	21%	61%	51%
Geese	17%	20%	26%	27%	51%	49%
Blue Wildebeest	26%	20%	43%	34%	82%	71%
Bighorn	31%	33%	46%	43%	71%	69%
Flatback Turtle	17%	25%	24%	37%	49%	65%
Green Turtle	29%	28%	44%	40%	73%	67%
Galapagos Sea Lion	31%	22%	43%	33%	73%	60%
Elephant Seal	23%	18%	33%	26%	56%	50%
Ship	23%	20%	36%	31%	65%	60%
Drifter	38%	30%	54%	45%	85%	80%

generalization [32] of the IMM to heterogeneous-order models (i.e., to models which share only some parts of their state vectors), random walks and CRWs will cooperate seamlessly. Second, by following the IMM smoother [33], location estimates will be computed from measurements gathered over a fixed interval, be these in the past, present, or future. Such enhancements will be proposed in forthcoming versions of the Argos processing chain.

ACKNOWLEDGMENT

The authors would like to thank all Argos users who kindly provided access to their data to qualify the new Kalman filter positioning algorithm presented here. The GPS drifters that provided the data used in the validation analysis were funded by Office of Naval Research Grant N00014-08-1-0557 and by National Oceanic and Atmospheric Administration Grant NA10OAR4320156.

REFERENCES

[1] B. McConnell, C. Chambers, K. Nicholas, and M. Fedak, "Satellite tracking of grey seals (Halichoerus grypus)," *J. Zoology*, vol. 226, no. 2, pp. 271–282, Feb. 1992.

[2] D. Austin, J. McMillan, and W. Bowen, "A three-stage algorithm for filtering erroneous Argos satellite locations," *Mar. Mammal Sci.*, vol. 19, no. 2, pp. 371–383, Apr. 2003.

[3] D. Douglas, *PC-SAS Argos Filter V5.0 Software Documentation*. Anchorage, AK, USA: U.S. Geol. Surv., Alaska Biological Science Center, 2000.

[4] S. Ferraroli, J. Georges, P. Gaspar, and Y. Maho, "Where leatherback turtles meet fisheries," *Nature*, vol. 429, no. 6991, pp. 521–522, Jun. 2004.

[5] Y. Tremblay, S. Shaffer, S. Fowler, C. Kuhn, B. McDonald, M. Weise, C. Bost, H. Weimerskirch, D. Crocker, M. Goebel, and D. P. Costa, "Interpolation of animal tracking data in a fluid environment," *J. Exp. Biol.*, vol. 209, no. 1, pp. 128–140, Jan. 2006.

[6] F. Royer and M. Lutcavage, "Filtering and interpreting location errors in satellite telemetry of marine animals," *J. Exp. Mar. Biol. Ecol.*, vol. 359, no. 1, pp. 1–10, Apr. 2008.

[7] I. Jonsen, J. Flemming, and R. Myers, "Robust state-space modeling of animal movement data," *Ecology*, vol. 86, no. 11, pp. 2874–2880, Nov. 2005.

[8] NGA, Springfield, VA, USA, World geodetic system, cited 2010. [Online]. Available: https://www.nga.mil/
[9] USGS, GTOPO30, cited 2010. [Online]. Available: http://www.usgs.gov/
[10] C. T. Kelley, "Iterative methods for optimization," in *SIAM Frontiers in Applied Mathematics*. Philadelphia, PA, USA: SIAM, 1999.
[11] *Argos User Manual*, CLS, Ramonville Saint-Agne, France, 2008.
[12] C. Kuhn, D. Johnson, R. Ream, and T. Gelatt, "Advances in the tracking of marine species: Using GPS locations to evaluate satellite track data and a continuous-time movement model," *Mar. Ecol. Progr. Ser.*, vol. 393, pp. 97–109, 2009.
[13] D. P. Costa, P. W. Robinson, J. P. Y. Arnould, A. Harrison, S. E. Simmons, J. L. Hassrick, A. J. Hoskins, S. P. Kirkman, H. Oosthuizen, S. Villegas-Amtmann, and D. E. Crocker, "Accuracy of Argos locations of pinnipeds at-sea estimated using Fastloc GPS," *PLoS ONE*, vol. 5, no. 1, p. e8677, Jan. 2010.
[14] M. Witt, S. Åkesson, A. Broderick, M. Coyne, J. Ellick, A. Formia, G. Haysf, P. Luschi, S. Stroud, and B. Godleya, "Assessing accuracy and utility of satellite-tracking data using Argos-linked Fastloc-GPS," *Animal Behav.*, vol. 80, pp. 571–581, 2010.
[15] R. E. Kalman, "A new approach to linear filtering and prediction problems," *Trans. ASME, J. Basic Eng.*, vol. 82, no. 1, pp. 35–45, Mar. 1960.
[16] H. W. Sorenson, *Kalman Filtering: Theory and Application*. Piscataway, NJ, USA: IEEE Press, 1985.
[17] S. Julier and J. Uhlmann, "A new extension of the Kalman filter to nonlinear systems," in *Proc. Int. Symp. Aerosp./Defense Sens., Simul. Controls*, 1997, vol. 3, pp. 183–193.
[18] E. Wan and R. Van Der Merwe, "The unscented Kalman filter for nonlinear estimation," in *Proc. IEEE AS-SPCC*, 2002, pp. 153–158.
[19] S. Julier, "The scaled unscented transformation," in *Proc. Amer. Control Conf.*, 2002, vol. 6, pp. 4555–4559.
[20] R. Van Der Merwe and E. Wan, "The square-root unscented Kalman filter for state and parameter-estimation," in *Proc. IEEE ICASSP*, Salt Lake City, UT, USA, 2002, vol. 6, pp. 3461–3464.
[21] E. Codling, M. Plank, and S. Benhamou, "Random walk models in biology," *J. Roy. Soc. Interface*, vol. 5, no. 25, pp. 813–834, Aug. 2008.
[22] X. Li and V. Jilkov, "Survey of maneuvering target tracking Part V: Multiple-model methods," *IEEE Trans. Aerosp. Electron. Syst.*, vol. 41, no. 4, pp. 1255–1321, Oct. 2005.
[23] H. Blom and Y. Bar-Shalom, "The interacting multiple model algorithm for systems with Markovian switching coefficients," *IEEE Trans. Autom. Control*, vol. 33, no. 8, pp. 780–783, Aug. 1988.
[24] Y. Bar-Shalom and H. Chen, "IMM estimator with out-of-sequence measurements," *IEEE Trans. Aerosp. Electron. Syst.*, vol. 41, no. 1, pp. 90–98, Jan. 2005.
[25] L. A. Hawkes, S. Balachandran, N. Batbayar, P. J. Butler, P. B. Frappell, W. K. Milsom, N. Tseveenmyadag, S. H. Newman, G. R. Scott, P. Sathiyaselvam, J. Y. Takekawa, M. Wikelski, and C. M. Bishop, "The trans-Himalayan flights of bar-headed geese (Anser indicus)," *Proc. Nat. Acad. Sci. USA*, vol. 108, no. 23, pp. 9516–9519, Jun. 2011.
[26] S. Benhamou, J. Sudre, J. Bourjea, S. Ciccione, A. De Santis, and P. Luschi, "The role of geomagnetic cues in green turtle open sea navigation," *PLoS ONE*, vol. 6, no. 10, p. e26672, Oct. 2011.
[27] S. Villegas-Amtmann, S. E. Simmons, C. E. Kuhn, L. A. Huckstadt, and D. P. Costa, "Latitudinal range influences the seasonal variation in the foraging behavior of marine top predators," *PLoS ONE*, vol. 6, no. 8, p. e23166, 2011.
[28] P. W. Robinson, D. P. Costa, D. E. Crocker, J. P. Gallo-Reynoso, C. D. Champagne, M. A. Fowler, C. Goetsch, K. T. Goetz, J. L. Hassrick, L. A. Hückstädt, C. E. Kuhn, J. L. Maresh, S. M. Maxwell, B. I. McDonald, S. H. Peterson, S. E. Simmons, N. M. Teutschel, S. Villegas-Amtmann, and K. Yoda, "Foraging behavior and success of a mesopelagic predator in the northeast Pacific Ocean: Insights from a data-rich species, the northern elephant seal," *PLoS ONE*, vol. 7, no. 5, p. e36728, May 2012.
[29] A. Dragon, P. Monestiez, A. Bar-Hen, and C. Guinet, "Linking foraging behaviour to physical oceanographic structures: Southern elephant seals and mesoscale eddies east of Kerguelen Islands," *Progr. Oceanogr.*, vol. 87, no. 1–4, pp. 61–71, Oct. 2010.
[30] A. Dragon, A. BarHen, P. Monestiez, and C. Guinet, "Horizontal and vertical movements as predictors of foraging success in a marine predator," *Mar. Ecol. Progr. Ser.*, vol. 447, pp. 243–257, Feb. 2012.
[31] X. Hoenner, S. D. Whiting, M. A. Hindell, and C. R. McMahon, "Enhancing the use of Argos satellite data for home range and long distance migration studies of marine animals," *PLoS ONE*, vol. 7, no. 7, p. e40713, Jul. 2012.
[32] R. Lopez, P. Danès, and F. Royer, "Extending the IMM filter to heterogeneous-order state space models," in *Proc. 49th IEEE Conf. Decision Control*, Dec. 2010, pp. 7369–7374.
[33] R. Lopez and P. Danès, "Exploiting Rauch–Tung–Striebel formulae for IMM-based smoothing of Markovian switching systems," in *Proc. IEEE ICASSP*, Kyoto, Japan, 2012, pp. 3953–3956.

Rémy Lopez received the M.S. degree in mathematical and modeling engineering and the Ph.D. degree in automatics from the National Institute for Applied Sciences, Toulouse, France, in 2009 and 2013, respectively.

He is currently with the Space Systems Department, Collecte Localisation Satellites, Ramonville-Saint-Agne, France. He was with the Laboratoire d'Analyse et d'Architecture des Systèmes, French National Center for Scientific Research (CNRS)/ Université Paul Sabatier, Université de Toulouse, Toulouse. His research interests include target tracking and statistical signal processing.

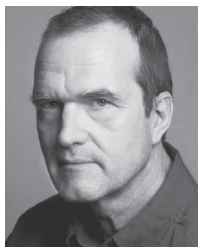

Jean-Pierre Malardé received the M.S. degree in physics and the Ph.D. degree in physics option remote sensing from the University of Paris VII (Paris Diderot University), Paris, France, in 1983 and 1991, respectively.

Between 1985 and 1990, he was a Project Engineer with the Groupement pour le Développement de la Télédétection Aérospatiale, Toulouse, France. He was involved in the algorithm and software development of the ERS-1 radar scatterometer processing. Since 1990, he has been with Collecte Localisation Satellites, Ramonville-Saint-Agne, France, where he is in charge of Argos localization processing and has been the Head of the Space Systems Department since 2010. He has been involved in different projects or studies as a Specialist in localization algorithms and system performance.

François Royer received the Eng. degree in agronomy and the Ph.D. degree in marine science from the École Nationale Supérieure Agronomique de Rennes, Rennes, France, in 2000 and 2005, respectively.

Between 2007 and 2012, he was a Research Engineer with Collecte Localisation Satellites, Ramonville-Saint-Agne, France, where he developed techniques for underwater positioning. He is the Founder of Datasio, Toulouse, France, which provides data mining software and services.

Philippe Gaspar (M'92) received the Eng. degree and the Ph.D. degree in applied mathematics from the Catholic University of Louvain, Louvain-La-Neuve, Belgium, in 1980 and 1985, respectively. He also received an Accreditation to supervise research from Université Paul Sabatier, Toulouse, France, in 2009.

Between 1985 and 1990, he held various research positions with the French National Centre for Meteorological Research (CNRM), the French National Center for Scientific Research (CNRS), and the Center for Meteorology and Physical Oceanography, Massachusetts Institute of Technology, Cambridge, MA, USA. In 1990, he became the Head of the Satellite Oceanography Division, Collecte Localisation Satellites, Ramonville-Saint-Agne, France, which he developed and led until 2006, where he is currently the Scientific Coordinator of this division. His main areas of expertise include oceanic turbulence modeling, satellite altimetry, stochastic optimal estimation, marine animal tracking and behavior modeling.